NECTIN-LIKE INTERACTIONS BETWEEN POLIOVIRUS AND ITS RECEPTOR TRIGGER CONFORMATIONAL CHANGES ASSOCIATED WITH CELL ENTRY

Supplemental Material -

Mike Strauss, David J. Filman, David M. Belnap, Naiqian Cheng, Roane T. Noel, and James M. Hogle

Cryo-Electron Microscopy and Three-dimensional Reconstruction to Moderate Resolution.

Frozen poliovirus-sPvr specimens were imaged as described previously (1). For poliovirus-sdPvr, frozen specimens were imaged at low electron dose on a CM200-FEG transmission electron microscope (FEI, Hillsboro, Oregon). Micrographs were recorded on Kodak SO-163 film. Micrographs were digitized on a SCAI scanner (Z/I Imaging, Huntsville, Alabama, USA) at a step size of 7.00 μm or on a Nikon Super Coolscan 9000 ED scanner (Tokyo, Japan) at a step size of 6.35 μm.

Individual poliovirus-sPvr and poliovirus-sdPvr particle images were extracted into 287x287-pixel boxes, and their corresponding contrast transfer function (CTF) parameters were determined and corrected by means of the program bctf in the Bsoft package (2). For determining orientation and origin parameters, particle images were corrected for phase reversals in the CTF. Images used for the final three-dimensional reconstructions were corrected for both phase reversal and decay (3). Pairs of images,

recorded at different defocus levels, were summed when determining particle orientations (3), but were not summed for origin determination or for three-dimensional reconstruction. Orientation and origin parameters for each particle image were determined using a modified version of the PFT algorithm (4), which was altered to include both phase and amplitude information in parameter refinement (5, 6). Three-dimensional reconstructions were computed with a Fourier-Bessel algorithm (7, 8) as implemented in EM3DR2. Size calibration of the virus-receptor reconstructions was carried out by comparing their radially averaged density plots (9) to that calculated from our previously reported cryoEM reconstructions of the poliovirus-sPvr complex (1). By design, the resulting size scale is consistent with a reconstruction of the poliovirus 160S particle (10),and matches low resolution electron density computed, as described previously (2, 11), from poliovirus atomic coordinates (PDB entry 1ASJ (12)). Given that the CTF is highly sensitive to the magnification, the good fit of capsid and receptor coordinates into the poliovirus-receptor reconstructions (Fig. 2C,2D) indicates that our choice of scale must be within acceptable tolerances. The resolution of each reconstruction was estimated by calculating a Fourier Shell Correlation (FSC) between two halves of each data set. The resulting FSC plots indicated agreement between half-set reconstructions to a resolution of ~9 Å (glycosylated: 9.6 Å and 8.8 Å, deglycosylated: 9.3 Å and 8.5 Å, according to 0.5 and 0.143 correlation criteria, respectively).

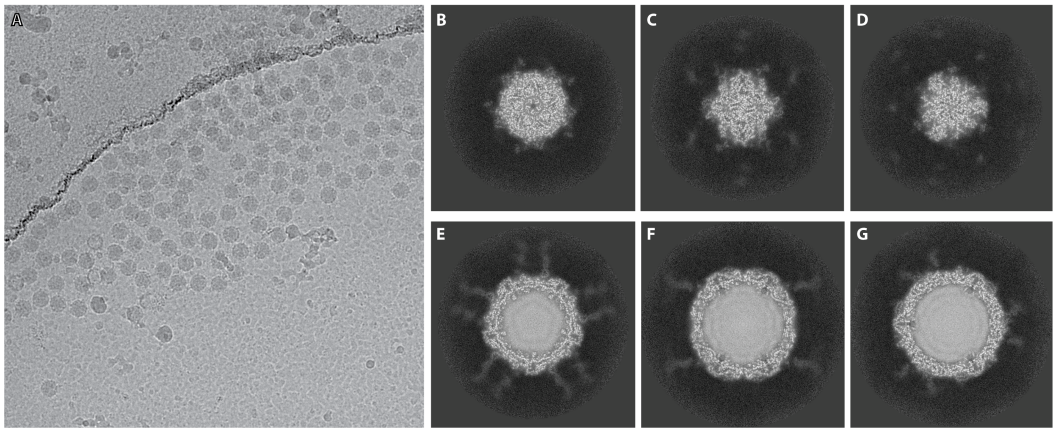

Supplemental Figure 1. A representative micrograph and sections through the final 4Å reconstruction. (A) A representative image of a field of receptor-decorated poliovirions. This image was recorded on a Gatan K2 Summit in super-resolution dose-fractionation mode, and represents the sum of aligned dose-fractionated frames. (B-D) 2Å slices close to the capsid surface are perpendicular to the 5-, 2-, and 3-fold axes, respectively. (E-G) 2Å slices through the 5-fold mesas when looking along the 5-, 2-, and 3-fold axes, respectively. Beta strands within beta sheets are clearly visible and well-separated.

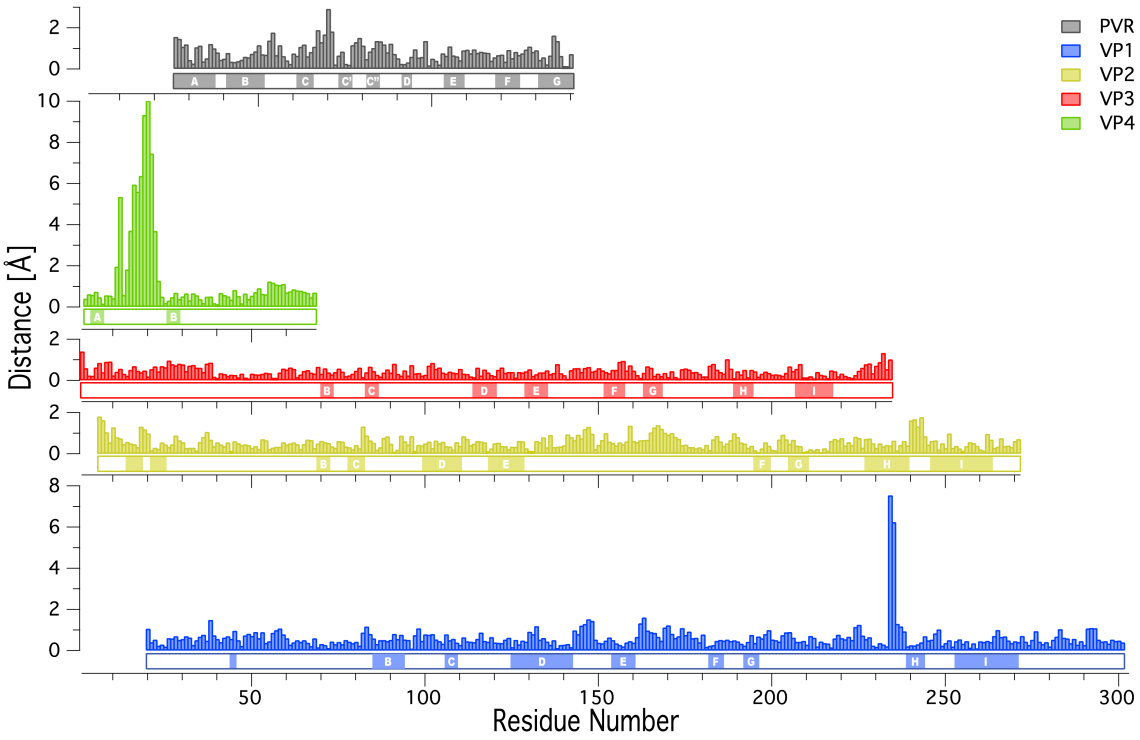

Supplemental Figure 2. Alpha carbon shifts that result from Pvr binding by poliovirus. For each polypeptide chain we have plotted the difference in alpha carbon position as a function of residue number. Reference models for comparison were obtained from the published poliovirus model (pdb: 1HXS) and from domain 1 of Pvr (pdb: 4FQP). The positions of beta strands in the protein sequence, are indicated by dark patches at the bottom of each plot and labeled by letter. These regular secondary structural elements are usually more constrained in their movement than the loops and terminal extensions. Pvr: grey, VP1: blue, VP2: yellow, VP3: red, VP4: green.

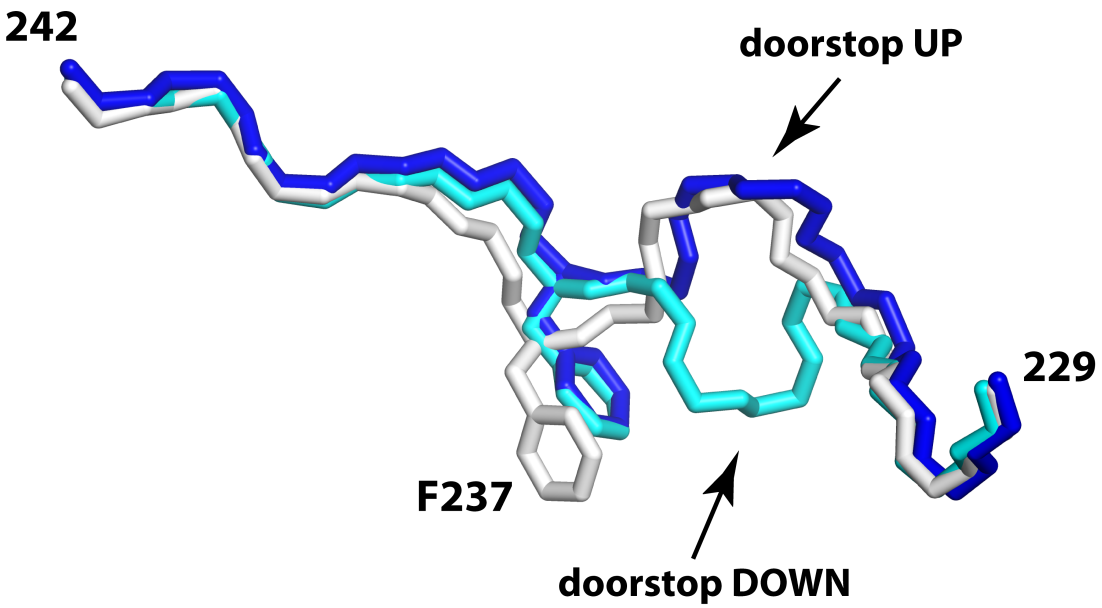

Supplemental Figure 3. Residues around the VP1 doorstop are seen in various conformations in different poliovirus structures. Atoms from the main chain of residues 229-242 are superimposed, with crystal structures 2PLV and 1HXS in blue and cyan, respectively, and our current model of the PV-sdPvr complex in white. Note that in native poliovirions, the “up” and “down” conformations of the doorstop (residues 233-236) do not affect the position of the Phe237 side chain. In contrast, the constrained conformation of the doorstop in the poliovirus-sdPvr complex forces the Phe237 side chain significantly more deeply into the middle of the VP1 beta barrel, where its position would conflict with “pocket factor”.

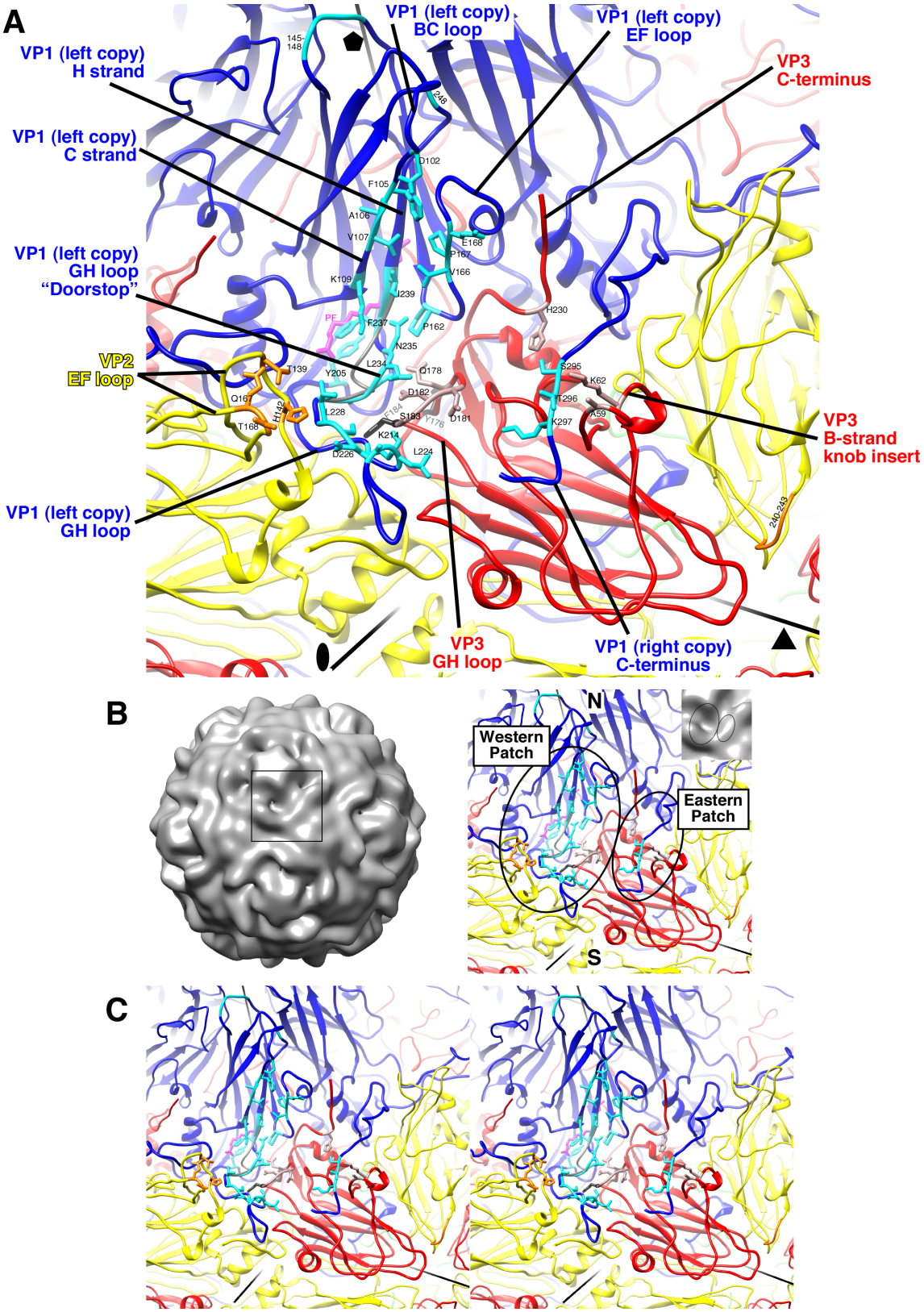
A
VP1 (left copy)
H strand
VP1 (left copy)
C strand
VP1 (left copy)
GH loop
"Doorstop"
VP2
EF loop
VP1 (left copy)
GH loop
VP1 (left copy)
BC loop
VP1 (left copy)
EF loop
VP3
C-terminus
VP3
B-strand
knob insert
VP3
GH loop
VP1 (right copy)
C-terminus
145-148
248
D102
F105
A106
V107
E168
P167
V166
K109
I239
H230
PE
F237
P162
N235
L234
T139
Y205
Q178
S295
K62
D182
T296
A59
Q161
H142
T168
L228
S183
Y178
D181
K297
K214
D226
L224
240-243
B
N
Western
Patch
Eastern
Patch
S
C

Supplemental Figure 4. "Footprint" of Pvr interaction on poliovirus. Surface capsid proteins in region near quasi-threefold axis (where VP1 and VP2 from one pentamer interact with VP3 from the pentamer to the right (as viewed from outside the capsid) are shown in ribbon representation. General color scheme: VP1, blue; VP2, yellow; VP3, red; VP4, green. Residues interacting with Pvr are shown as stick diagrams and are colored cyan (VP1), orange (VP2), and light red (VP3). Otherwise, no side chains are shown. All residues shown are from our model, except the native virus region at the "doorstop" (gray wire) and the native pocket factor modeled as palmitic acid (magenta), which is absent in our high-resolution map. Compare to Suppl. Tables 1 and 2.

A. Interacting regions are identified by secondary structure (cf. Supplemental Table 1 and 2). Symmetry axes (black lines radiating from center of capsid) are labeled as twofold (oval), threefold (triangle), and fivefold (pentagon).

B. (Left) Same view as panel A but with "western" and "eastern" contact patches identified. "North" and "south" positions are also shown. (Right) Surface rendering of native poliovirus (10). A box shows the area of a single Pvr binding site that is shown in the other panels. Symmetry axes are present, but are unlabeled (see panel A).

C. Stereo representation of the Pvr "footprint" on poliovirus without labeling.

Supplemental Table 1. Important intermolecular contacts that stabilize the poliovirus-Pvr complex at 4°C (cf. Suppl. Fig. 4).

Contact Patch	Poliovirus					Interaction^	Pvr (D1)			
	chain	region	residue	atom*	mutation§		region	residue	atom*	mutation§
Eastern										
SE corner	VP1 (right copy)	C-terminus	Lys297	NZ		H-bond	C"D loop	Ser87	O	A87 [16,18], P87 [19]
			Thr296	OG1		H-bond		Glu88	OE2	A88 [18], N88 [19]
E edge			Thr296	side chain		proximity	CC' loop	Arg68	NH2	
			Ser295	OG	Pro293, Ser295 [14]	H-bond		Gly73	N	A73 [18], T73 [19]
	VP3	B-strand knob insert	Lys62	NZ		salt link	CC' loop	Glu71	OE2	A71 [18], D71 [19]
			Ala59	CB	Ala59 [14]	hydrophobic	EF loop	Glu116	CB	A116 [18], D117[17,19], D177F [16]
			Ala59	CB	Ala59 [14]	hydrophobic		Arg114	NH1	E114 [18]
NE corner		C-term.	His230†	CA		hydrophobic	CC' loop	Ser72	OG	A72 [18], G72 [19]
Western										
NW corner	VP1 (left copy)	BC loop	Asp102	OD2	type differences [17]	salt link	G strand	Arg133	NH1	
		EF loop‡	Val166	CG2	H166 [16]	proximity		Phe128	CE1	G130,H130,A131 [18]; N130,T132 [19]
			Val166	O	H166 [16]	H-bond		Ser132	OG	T132 [19]
			Pro167	O		H-bond		Ser134	N	R134 [19]
			Glu168	OE2	G168 [15,16]	H-bond		Ser134	OG	R134 [19]
		C-strand	Phe105	side chain	M105,T105 [20]	hydrophobic	FG loop	Gly131	CA	A131 [18]
			Ala106	CA		proximity		Pro129	CB	
			Val107	O	M107 [16]	vanderWaals		Phe128	CD1	A128 [18]
			Val107	CG2	M107 [16]	proximity		Gly131	CA	A131 [18]
			Val107	O	M107 [16]	vanderWaals		Phe128	side chain	A128 [18]
			Lys109	CB	R109 [16]	hydrophobic		Phe128	CD1	A128 [18]
		H-strand	Ile239	side chain	type differences, S239, V239 [12]	hydrophobic		Phe128	side chain	A128 [18]
W edge		Doorstop	Leu234	CD1	P234 [14]	hydrophobic	C'C" loop	Thr81	CA, O	S81 [19]
		GH loop	Ala232	O		H-bond		Gln82	NE2	A82 [18], F82 [19]
	VP3	GH loop#	Asp182	OD1		H-bond		Gln82	NE2	A82 [18], F82 [19]
SW corner	VP1 (left copy)	GH loop	Ala231	CB	V231 [14]	hydrophobic	C'C" loop	Thr81	CB	S81 [19]
			Leu228	CD1	F228 [14]	hydrophobic		Thr81	CA	S81 [19]
			Leu228	N	F228 [14]	H-bond		Thr81	O	S81 [19]
			Ser213	side chain		proximity		Gln82	side chain	A82 [18], F82 [19]
			Lys214	NZ	R214 [16]	H-bond		Gln82	O	A82 [18], F82 [19]
			Asp226	CG	G226,N226 [14]; E226,A226 [16]	hydrophobic		Leu99	CD1	A99 [16,18], T99 [19]
			Ser227	N		hydrophobic	DE loop	Leu99	CD1	A99 [16,18], T99 [19]
	VP3	GH loop#	Ser183	OG	G183 [14]; R183 [15]	hydrophobic	C'C" loop	Gln82	CB	A82 [18], F82 [19]
	VP2	EF loop	Thr139	OG1		H-bond	DE loop	Gly100	O	A100 [16,18], N100 [19]
			His142	side chain	Y142 [12,13,15]; F142 [13]	hydrophobic		Leu99	CB	A99 [16,18], T99 [19]
			Gln167	O	A167 [16]	hydrophilic		Arg98	NH1,NH2	A98 [18]
			Gln168	O	G168 [15]	hydrophilic		Arg98	NH1,NH2	A98 [18]

Contact Patch	Poliovirus					Interaction^	Pvr (D1)			
	chain	region	residue	atom*	mutation§		region	residue	atom*	mutation§
S edge	VP1	GH loop (distal end)¶	Ala223	CB		hydrophobic	C" strand	Pro84	N,CG	H84 [16,18], V84 [19]
			Leu224	CD1		hydrophobic		Tyr86	CD1	G86[16], S86[16,18], A86[18], F86[19]
			Leu224	CD1		hydrophobic		Ser89	OG	
	VP3	GH loop#	Asp181	O	N181 [15]	proximity	C'C" loop	His79	NE2	

*Protein Data Bank file designation.

§The mutational data mentioned in this table come from references 12–20. Some of those papers discuss specific mutation of several other poliovirus or Pvr residues which affected poliovirus binding or replication, but those residues were not identified in our study as being directly involved in virus-receptor interactions at 4°C. Some differences labeled "mutations" here are sequence differences between the three types of poliovirus.

^Hydrophilic/Proximity indicates a lack of good geometry for hydrogen bonding.

†His230 is part of a putative zinc-binding site.

‡During expansion to the 135S form, EF loop moves with respect to core jelly roll.

#GH loop of VP3 rearranges upon expansion to the 135S state.

¶Distal end of VP1 GH loop disorders upon expansion to the 135S state.

Supplemental Table 2. Poliovirus-poliovirus "doorstop" interactions induced or enhanced by interactions with Pvr (at 4°C)

VP1 Doorstop			Interaction^	Interacting				
residue	**atom***	**mutation**		**chain**	**region**	**residue**	**atom***	**mutation**
Lys214	NZ	Arg214 [16]	H-bond	VP3	GH loop	Ser183	OG	Gly183 [14], Arg183 [15]
Ser233	OG		H-bond			Gln178	NE2	Leu178,Arg178 [14,20]
Leu234	N	Pro234 [14]	H-bond			Asp182	OD2	
Leu234	O	Pro234 [14]	H-bond	VP1	C-strand	Lys109	NZ	Arg109 [16]
Asn235	OD1		H-bond		H-strand	Gly238	N	
Asn235	ND2		proximity		EF loop	Pro162	CA	Gly162 [16]
Asp236	O		proximity		EF loop	Pro162	CG	Gly162 [16]

*These interactions stabilize the "super-up" conformation of the doorstop.

^Proximity indicates a lack of good geometry for hydrogen bonding.

References

1. **Belnap DM, McDermott BM, Jr., Filman DJ, Cheng N, Trus BL, Zuccola HJ, Racaniello VR, Hogle JM, Steven AC.** 2000. Three-dimensional structure of poliovirus receptor bound to poliovirus. Proceedings of the National Academy of Sciences of the United States of America **97:**73-78.
2. **Heymann JB, Belnap DM.** 2007. Bsoft: image processing and molecular modeling for electron microscopy. J Struct Biol **157:**3-18.
3. **Conway JF, Steven AC.** 1999. Methods for reconstructing density maps of "single" particles from cryoelectron micrographs to subnanometer resolution. J Struct Biol **128:**106-118.
4. **Baker TS, Cheng RH.** 1996. A model-based approach for determining orientations of biological macromolecules imaged by cryoelectron microscopy. J Struct Biol **116:**120-130.
5. **Bubeck D, Filman DJ, Cheng N, Steven AC, Hogle JM, Belnap DM.** 2005. The Structure of the Poliovirus 135S Cell Entry Intermediate at 10-Angstrom Resolution Reveals the Location of an Externalized Polypeptide That Binds to Membranes. J Virol **79:**7745-7755.
6. **Sanz-Garcia E, Stewart AB, Belnap DM.** 2010. The random-model method enables ab initio 3D reconstruction of asymmetric particles and determination of particle symmetry. J Struct Biol **171:**216-222.
7. **Crowther RA, Amos LA, Finch JT, De Rosier DJ, Klug A.** 1970. Three dimensional reconstructions of spherical viruses by fourier synthesis from electron micrographs. Nature **226:**421-425.
8. **Fuller SD, Butcher SJ, Cheng RH, Baker TS.** 1996. Three-dimensional reconstruction of icosahedral particles--the uncommon line. J Struct Biol **116:**48-55.
9. **Belnap DM, Grochulski WD, Olson NH, Baker TS.** 1993. Use of radial density plots to calibrate image magnification for frozen-hydrated specimens. Ultramicroscopy **48:**347-358.
10. **Belnap DM, Filman DJ, Trus BL, Cheng N, Booy FP, Conway JF, Curry S, Hiremath CN, Tsang SK, Steven AC, Hogle JM.** 2000. Molecular tectonic model of virus structural transitions: the putative cell entry states of poliovirus. J Virol **74:**1342-1354.
11. **Belnap DM, Kumar A, Folk JT, Smith TJ, Baker TS.** 1999. Low-resolution density maps from atomic models: how stepping "back" can be a step "forward". J Struct Biol **125:**166-175.
12. **Wien MW, Curry S, Filman DJ, Hogle JM.** 1997. Structural studies of poliovirus mutants that overcome receptor defects. Nat Struct Biol **4:**666-674.
13. **Colston EM, Racaniello VR.** 1995. Poliovirus variants selected on mutant receptor-expressing cells identify capsid residues that expand receptor recognition. J Virol **69:**4823-4829.
14. **Colston E, Racaniello VR.** 1994. Soluble receptor-resistant poliovirus mutants identify surface and internal capsid residues that control interaction with the cell receptor. The EMBO journal **13:**5855-5862.
15. **Liao S, Racaniello V.** 1997. Allele-specific adaptation of poliovirus VP1 B-C loop variants to mutant cell receptors. J.Virol. **71:**9770-9777.

16. **Harber J, Bernhardt G, Lu HH, Sgro JY, Wimmer E.** 1995. Canyon rim residues, including antigenic determinants, modulate serotype-specific binding of polioviruses to mutants of the poliovirus receptor. Virology **214:**559-570.
17. **Filman DJ, Syed R, Chow M, Macadam AJ, Minor PD, Hogle JM.** 1989. Structural factors that control conformational transitions and serotype specificity in type 3 poliovirus. EMBO J. **8:**1567-1579.
18. **Bernhardt G, Harber J, Zibert A, DeCrombrugghe M, Wimmer E.** 1994. The poliovirus receptor: Identification of domains and amino acid residues critical for virus binding. Virology **203:**344-356.
19. **Aoki J, Koike S, Ise I, Sato-Yoshida Y, Nomoto A.** 1994. Amino acid residues on human poliovirus receptor involved in interaction with poliovirus. J.Biol.Chem. **269:**8431-8438.
20. **Macadam AJ, Arnold C, Howlett J, John A, Marsden S, Taffs F, Reeve P, Hamada N, Wareham K, Almond J, Cammack N, Minor PD.** 1989. Reversion of the attenuated and temperature-sensitive phenotypes of the Sabin type 3 strain of poliovirus in vaccinees. Virology **172:**408-414.